Macromolecules

ARTICLE

pubs.acs.org/Macromolecules

Cavitation and Crazing in Rod-Containing Nanocomposites

Gregory N. Toepperwein and Juan J. de Pablo*

Department of Chemical and Biological Engineering, University of Wisconsin, Madison, Wisconsin 53706-1691, United States

ABSTRACT: Addition of nanoparticles to a polymer can drastically affect the mechanical properties and structure of the nanocomposite. Here we investigate the nucleation and growth of voids that precede craze formation and the early crazing itself by use of coarse-grained Monte Carlo and molecular dynamics simulations. We investigate the role of deformation rate, local density, local rod orientation, nonaffine displacements, and local elastic moduli. We observe that for both pure polymers and nanocomposites, regions of low local elastic modulus are more prone to failure. Additionally, it is found that Voronoi volume can anticipate void formation and that it is also a predictor of failure, particularly in composites. After the onset of crazing, it is found that nanorods incorporated into the crazes rapidly orient themselves to match the direction of the polymer fibrils, but nanorods in bulk regions remain randomly oriented. We further find that attractive rods resist incorporation into the developing crazes and that this effect is stronger with increasing rod length.

INTRODUCTION

Crazing is a unique mode of failure for polymeric materials during which a strong dilatational component induces a rapid volume gain before failure. Before global failure can occur, a region of organized fibrils, or tendrils, of polymer material forms. Tendrils can be on the order of several hundred nanometers in length. This process requires significant energy, making it a source of the toughness of polymeric materials that is so vital to their use in load-bearing applications.

Cavitation of a polymer melt is a requisite for crazing.[1,2] The mechanisms of initial void formation are unclear, but previous work suggests that regions of high local mobility[3] or material defects, such as chain ends or repulsive filler materials, could serve as nucleation points. At present, it is not possible to predict the location of void formation in polymeric materials.

Kramer and Berger[4] used small-angle X-ray scattering to examined propagating crazes. Their model predicted that capillary forces drive the shape and distribution of forming fibrils, from which one would expect surface tension to be the dominant contributor to stress. Estevez et al.[5] examined the fracture toughness of homogeneous glassy polymers via constitutive equations to investigate the competition between shear yielding and crazing. They noted that the development of crazes depended upon the kinetics of local plastic deformation. Mahajan et al.[1] examined the evolution of the entanglement state during the early stages of crazing. Using a coarse-grained, bead−spring polymer model, they produced well-equilibrated polymer melts and then subjected them to strain in one dimension with the cross-sectional area held constant. Those authors found that the number of total topological constraints remained relatively constant during crazing but that these constraints moved away from the crazing material and into the undeformed bulk. Rottler and Robbins conducted an investigation of the early behavior of pure polymer crazes using a similar model.[6] They found that the characteristic length of stretched chains is one-third the entanglement length and that the drawing stress of the system is carried primarily by covalent bonds. This is in conflict with older capillary models[4] for craze development, which predict most of the stress to be associated with surface tension.

While the molecular origins and dynamic development of crazes have received considerable attention, attempts to extend the current understanding to nanocomposite materials have been limited. The addition of nanoparticles can drastically influence the properties of polymeric materials. Polymer nanocomposites (PNCs) are increasingly important, with applications ranging from flame-retardant fabrics to aircraft hulls. It is now appreciated that changes to polymer behavior depend on numerous additive properties[7−11] including particle concentration, particle geometry, particle size, interfacial interactions, and thermal history. However, nanoparticle influence upon material failure via crazing remains poorly understood.

Lee et al.[12] demonstrated a fundamentally different behavior in craze development upon the addition of surface-modified cadmium selenide to polystyrene. Whereas pure polymer crazes transition smoothly from a small void to a mature craze followed by a crack tip, PNC crazes experience a premature phase during which small pockets of additive rich bulk become temporarily trapped between developing crazes before eventually aggregating and organizing into a mature craze. Bagheri and Pearson[13] experimentally examined rubber-toughened epoxies and found that cavitation resistance of the rubber phase did not contribute to the toughness of the epoxy, indicating that the makeup of the additive was less important than the fact that it was physically present. They also suggested that cavitation resulted from a local reduction in bulk modulus. By use of molecular dynamics simulations, Gersappe[14] found that nanofillers increased toughness and that additive mobility helped dissipate energy.

Received: March 14, 2011
Revised: May 16, 2011
Published: June 07, 2011

The nature of local mechanical properties is important to the understanding of systems undergoing extreme deformation. Yoshimoto et al.[15] calculated the local elastic moduli of polymeric glasses by a stress-fluctuation approach and demonstrated that such materials are mechanically heterogeneous at small length scales. Buryachenko et al.[16] used measurements of local mechanical properties to study how an applied force propagated though a material but did not comment on failure directly. Papakonstantopoulos et al.[17] extended the work of Yoshimoto to the examination of nanocomposites and demonstrated that the polymer near an attractive inclusion exhibits improved local elastic moduli as compared to the polymer in the matrix. Papakonstantopoulos et al.[18] were later able to examine local mechanical properties at the level of individual monomers and demonstrated that sites having small elastic moduli are most prone to failure. Together, such studies have clearly established that there is a strong correlation between local elastic moduli and the type of nonaffine plastic failure that is otherwise associated with polymer glass deformation.

In the present work, we take the work of Papakonstantopoulos et al. a step further and use simulations to examine the formation of voids and early stages of crazing in pure polymers and PNCs. The development of a crack tip propagating ahead of a mature craze and subsequent failure of the material are processes beyond the scope of the current work. We examine the influence of particle geometry by examining particles of varying length. To understand void formation, we examine the local mechanical properties of PNC systems. We find that voids form preferentially in regions of low local elastic modulus and that these regions can be identified by examining Voronoi volumes for PNCs. We also find that the addition of attractive nanoparticles induces earlier void formations due to a more mechanically heterogeneous environment. In the developing crazes, we find that larger particles resist incorporation into developing voids, consistent with the trapped regions of additive found experimentally by Lee et al.[12]

MODEL AND METHODS

Melts of fully flexible polymer chains are modeled using a coarse-grained bead−spring model. Nanorod additives consisting of 4 or 8 beads are incorporated into this polymer matrix at a concentration of 10 wt %. For convenience, PNC systems are referred to by the length of their inclusions (i.e., 4-mer and 8-mer). Nonbonded interactions are governed by a Lennard-Jones potential with a cutoff of 2.5σ, where σ and ε are the Lennard-Jones length and energy units, respectively. This potential is smoothed between 2.4σ and 2.5σ so that both the potential and force go to zero at the cutoff. Both polymer and particle beads have a diameter of σ. Particle−particle and polymer−polymer nonbonded interactions have a characteristic energy of ε, while the particle−polymer nonbonded interaction has a characteristic energy of 3ε in order to provide an energetic driving force for the dispersion of inclusions. Molecular connectivity is enforced in both polymer and inclusions through the use of simple harmonic bonds, but rods have smaller equilibrium bond lengths than the polymer. Nanorods also have an additional harmonic angle potential to enforce a nearly linear conformation, but note that the rods are not strictly rigid. Full details of the potential forms and constants are described elsewhere.[19] The equilibrium structure, entanglement state, and response to uniaxial strains for this model have been previously characterized.[19,20]

Table 1. Number Density at Various Temperatures[a]

	number density at various temperatures		
system	density at $T = 1.2$	density at $T = 0.3$	glass transition temperature
pure polymer	0.808	1.026	0.39
4-mer	0.907	1.064	0.48
8-mer	0.905	1.069	0.42

[a] All density values are ± 0.002 and glass transition temperatures are ± 0.02.

The temperature (T), pressure (P), and time (t) are presented in reduced units of kT/ε, $\sigma^3 P/\varepsilon$, and $(\varepsilon t^2/m\sigma^2)^{1/2}$, respectively. Here, m is the mass of a bead and k is the Boltzmann constant. Time in reduced units will be denoted as τ.

For the present work, pre-equilibrated configurations of 4-mer, 8-mer, and pure polymer at a temperature of 1.75 were used to construct systems of 102 240 beads (for PNCs) or 162 000 beads (for the pure polymer). These systems had a $1 \times 2 \times 2$ box dimension ratio, the narrow dimension of which will be referred to as the x-dimension. Three independent configurations for each system were equilibrated to a new temperature of 1.2 at zero pressure for 10000τ. The LAMMPS bondswap algorithm,[21] which relies on connectivity altering moves,[22,23] was active during this equilibration to aid in the relaxation of polymer chains. This additional equilibration ensured that the density of the polymer relaxed to the new temperature.

After equilibration, each system was cooled from a temperature of 1.2 to 0.3 over the course of 900τ. The glass transition temperature was obtained by fitting lines to the high temperature and low temperature regimes of a density versus temperature plot; their intersection identified the glass transition. The samples were then aged 1000τ at constant pressure. The densities of the system before cooling and after aging are reported in Table 1.

While debate remains about the exact stress state required to induce cavitation and eventual crazing, Baljon and Robbins demonstrated that application of a triaxial stress reliably produced crazes.[2] To that end, samples were extended in the x-direction at a constant true strain rate of 7.3×10^{-4}, while the cross-sectional area of the sample was held constant for 1500τ. This process resulted in a positive effective stress in all directions, while allowing control of the dimension in which craze fibrils form. To more closely explore the early stages of void formation, less extreme deformations were independently performed at a lower strain rate of 1.2×10^{-4} for 1000τ. Additional analysis was performed at strain rates of 1.2×10^{-3} for 100τ and 1.2×10^{-5} for 10000τ to test the strain rate dependence of void formation.

The structure of forming voids was monitored by finding the Voronoi volume of all sites. The Voronoi volume measures the local space in the system that "belongs" to each site. In the present work, Voronoi volume was calculated by using the software package voro++.[24]

The origins of void formation were studied, in part, by calculation of the local elastic moduli (C) for each bead in the system during the course of deformation following the procedures outlined by Papakonstantopoulos et al.[18] For completeness, a brief overview of the main points is given here; for complete details, readers are referred to the literature. To determine C, we

use the definition of local elastic modulus for a single bead, namely

$$C_{ijkl} = \frac{\delta\sigma_{ij}}{\varepsilon_{kl}} \quad (1)$$

where $\delta\sigma$ denotes change in stress, ε denotes strain, and C denotes the local elastic modulus. The indexes i through l denote a set of the x, y, z vector components. To reduce noise associated with unimportant vibrations, each configuration of interest is minimized using the FIRE algorithm,[25] rescaled by 1.001 in the x-direction, and minimized again. This minimization allows measurement of the mechanical stiffness of the inherent structure. We focus explicitly on the tensile modulus in the x-direction, C_{xxxx}. Following our previous work, local stress was calculated via the site-based methodology of Zhou[18,26] according to

$$\sigma_{ij} = \frac{1}{2V} \sum_{\text{neighbors}} f_i r_j \quad (2)$$

where f_i is force on the reference bead in the ith direction, r_j is the distance to the bead causing the force in the jth direction, and V is the local volume around the bead. The local volume can be estimated either by treating the system as approximately uniform and dividing all system volume up equally among the sites or the Voronoi volume can be used. For this study we use the Voronoi volume from the minimized structure.

Following our previous work,[18] the definition of local strain provided by Falk and Langer is adopted.[27] Under this definition, the local strain can be found by performing a minute deformation and finding the strain tensor that best describes the local motion of the nearby particles. The optimal strain tensor can be calculated by finding the affine displacement that most closely resembles the actual displacements of neighboring molecules. In practice, three challenges arise from this method. First, when considering local neighbors, the farther away a site is, the more strongly its motion affects the outcome of the optimization. As such, only a relatively small set of particles about the site of interest can be considered, lest the outermost sites dominate the results, making the quantity not especially "local" in character. For this study, sites within 2.5σ of the reference particle are considered. Second, such measurements exhibit a large noise-to-signal ratio. The two minimized structures are used to calculate the local stress and strain so that changes to the mechanical state of the inherent structure are measured. Third, interpretation of this quantity for a bead on the interface of a forming void is difficult. Sites that constitute the polymer fibril in a craze see negligible local rearrangements, thereby obscuring measurement of local mechanical stiffness. As such, we will limit our use of local strain to systems of near-uniform density and hence to the earliest stages of void formation.

We further characterize the dynamics of the systems by measuring the evolution of nonaffine displacement fields during cavitation and crazing. An affine deformation is one in which all components move according to the macroscopic strain of the system. The nonaffine displacements simply measure how much each particle's movement deviates from the affine. We have previously used nonaffine displacements to demonstrate the heterogeneity of glassy systems and shown that this measure is correlated with to regions of low C.[18,28]

To quantify the connection between these measured properties, the Pearson product-moment correlation coefficient was

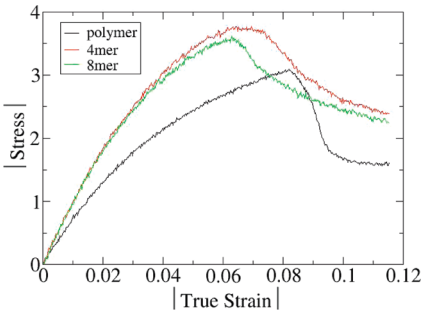

Figure 1. Triaxial deformation at a strain rate of 1.2×10^{-4}. The black line represents the pure polymer, the red line represents the 4-mer nanocomposite, and the green line represents the 8-mer nanocomposite.

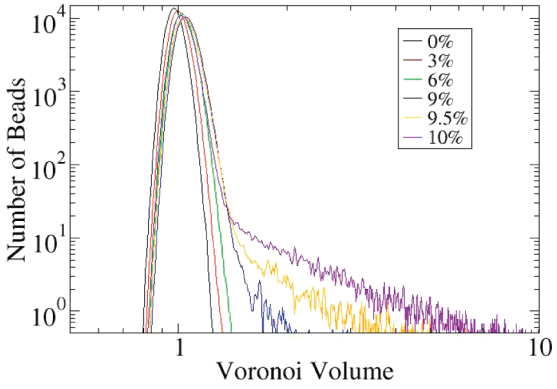

Figure 2. Distribution of Voronoi volume in pure polymer during triaxial deformation at a rate of 1.2×10^{-4}. Different lines correspond to different values of the percent true strain.

calculated according to

$$\rho_{X,Y} = \frac{E[(X-\overline{X})(Y-\overline{Y})]}{\sqrt{E[(X-\overline{X})^2]E[(Y-\overline{Y})^2]}} \quad (3)$$

where the operator E denotes the expected value of its operand, X and Y are the two properties whose correlation is being measured, and $\overline{X}$ and $\overline{Y}$ are the average values of X and Y, respectively. The normalized correlation (ρ) ranges in value between -1 and 1. A value of -1 corresponds to a complete negative linear correlation, and a value of 1 corresponds to a complete positive linear correlation; a value of 0 implies a lack of correlation.

It is important to note that this correlation is neither distributionally robust nor outlier resistant. In particular, as the measure of C in this work is dependent upon division by a local strain, which can be near zero, the outliers produced in C are problematic. As such, the top and bottom 1% of data for correlations involving C are excluded. This type of correlation measurement is appropriate when comparing, for example, two continuous properties that can be measured on a site-by-site basis. However, the existence of a void is not a property tied directly to a single site. A site-based definition, such as sites that border voids, is also problematic as the population will not exhibit the Gaussian-like distribution expected by a Pearson correlation. To that end, other variables are used for "voidness" when measuring some correlations.

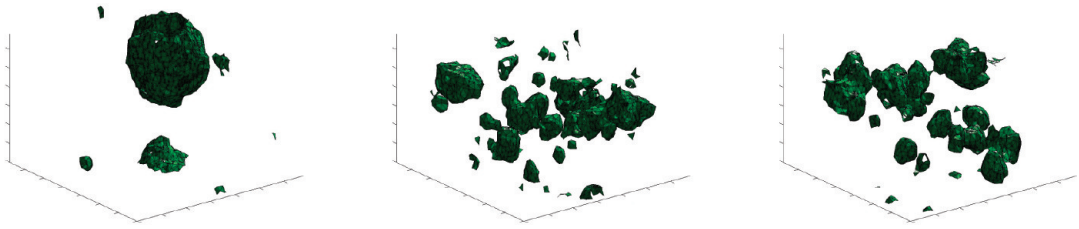

Figure 3. Visualization of voids on the basis of Voronoi volume for polymer, 4-mer, and 8-mer (from left to right) at 10% strain.

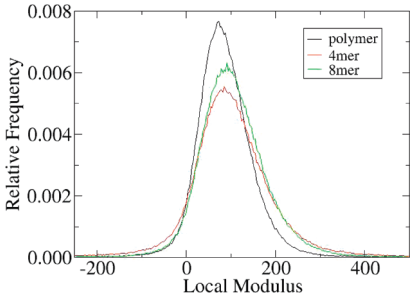

Figure 4. Distribution of local elastic modulus prior to deformation. The black line represents the pure polymer, the red line represents the 4-mer nanocomposite, and the green line represents the 8-mer nanocomposite. Values are for polymer component only.

Lastly, crazes demonstrate a characteristic extension ratio (λ) given by the polymer density of the undeformed region divided by the density of the crazed region. Approximating the entangled state of a polymer craze as a cross-linked system connected by random-walk segments, it can be shown that λ is related to the entanglement length (N_e) by

$$N_e = \frac{\lambda^2 {R_e}^2}{2(N-1){l_0}^2} \quad (4)$$

where ${R_e}^2$ is the polymer mean-squared end-to-end distance, N is the number of sites in the polymer, and l_0 is the average bond length. Despite simulation evidence that the characteristic length scale of crazed polymers is actually $N_e/3$,[6] for pure polymers this simple model relating λ to N_e has proven to be consistent with experiment.[29]

CAVITATION

Application of multiaxial stress led to cavitation and eventual crazing in all systems studied here. The stress−strain response of these systems is shown in Figure 1. For systems undergoing triaxial tension, one can observe a sharp stress peak and yield at relatively low strain, followed by a stress plateau. The pure polymer experiences a stress peak near 8% strain with a stress value slightly above three. Despite some model differences, this is in good qualitative agreement with previous work.[2] For the nanocomposites, it is observed that the stress peak occurs at lower values of strain and higher values of stress. After the stress peak, the stresses plateau more gradually for PNCs than for the pure polymers. The 4-mer provides better overall strengthening than the 8-mer, as the stress peak occurs at both a higher stress and a higher strain. We will see momentarily that this stress peak corresponds to the nucleation of incipient voids.

In order to characterize the nature of void formation, a metric must be identified to quantify the existence and location of voids. Prior to deformation, the Voronoi volume of a polymer site has a value around unity for the systems considered here.

For the pure polymer, the evolution of the distributions of Voronoi volume of sites is shown in a log−log plot in Figure 2. The undeformed system (black line) exhibits a Gaussian distribution that slowly widens and moves to higher values as the box is strained. At around 9% deformation a non-Gaussian tail begins to emerge. This tail corresponds to a small population of high-Voronoi-volume beads, i.e., sites that border regions of open space. It will be shown later that these sites correspond to the shell of beads that surround a nascent void. Once this tail begins to form, the Gaussian distribution describing the majority of the beads stops moving to the right, and instead the tail grows as a small number of sites take on all additional volume in the system created by further deformation. By the time the system has reached 10% deformation, the distribution describing the majority of beads has moved left, back to where it was at 6% deformation, while the tail continues to grow.

The overall volume of the samples increases with the length of the x-dimension of the box during deformation. Originally this volume is apportioned uniformly among all of the sites in the system, until a sufficient driving force exists to nucleate one or more voids. Once this void is formed, not only does it capture any further volume added to the system but it also takes on some of the additional volume previously held by the bulk, so that the majority of the system can relax down to a tighter packing. Specifically, nonvoid sites return to the volume they had at 6% deformation.

While there is no unique definition of a void, it can be seen from the polymer Voronoi volume distributions in Figure 2 that a prominent tail of high-volume beads appears around a value of 1.2. In what follows, sites with a Voronoi volume over 1.2 shall be described as large Voronoi volume sites (LVVS). Note that such LVVS occur even at equilibrium, as transient fluctuations that are clearly not part of a void, but those sites maintain their large Voronoi volume for only a few time steps. In systems with voids, the same LVVS will persist indefinitely.

Voids can be visualized by finding sets of three LVVS that are all within 2.5σ of each other and then drawing a triangle in space between the three points. These triangles outline clear shells around forming voids, with few spurious triangles arising due to random fluctuations. In the case of the pure polymer, a single large void tends to dominate the material. A representative single-void-dominated polymer system is shown in Figure 3. In the case of PNCs, multiple voids are formed throughout the system.

The distribution of C for the polymer component only is shown in Figure 4. As mentioned before, considerable variability

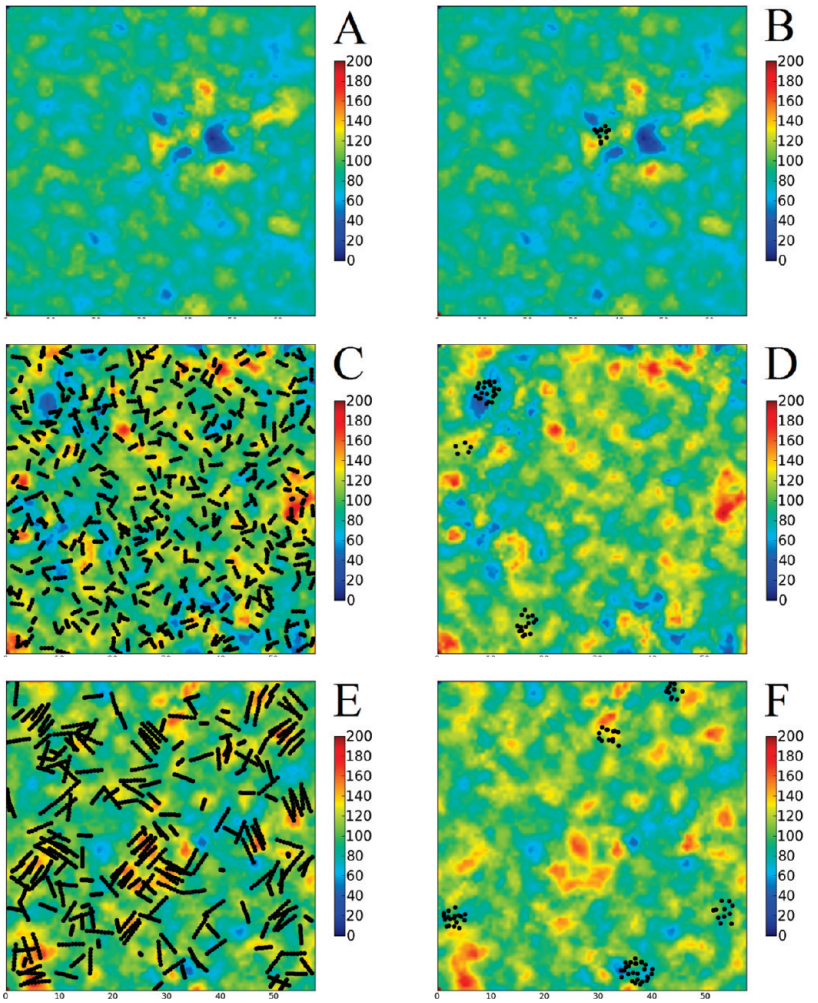

Figure 5. Cross section of local elastic (bulk) modulus corresponding to 4σ thick slices prior to deformation. Images A and B correspond to the pure polymer, images C and D correspond to the 4-mer nanocomposites, and images E and F correspond to the 8-mer nanocomposites. Images C and E are overlaid with position of rods, and images B, D, and F are overlaid with the location of early void formation sites. Superimposed void locations are from 9% deformation (polymer) and 7% deformation (PNCs).

exists in local moduli, corresponding to the heterogeneous nature of polymer glasses.[15] It can be seen that the distribution of local moduli is on average higher for PNCs. The median local moduli for the pure polymer, 4-mer, and 8-mer are 82.3, 97.9, and 99.5, respectively. The standard deviations of the Gaussian part of the distributions (e.g., fitting a Gaussian curve that ignores tails) are 51.4, 68.0, and 63.2, respectively. In the case of the 4-mer, the additional widening of the distribution leads to more regions of low moduli than seen in the pure polymer.

To understand why certain sites fail, it is useful to examine the local elastic moduli spatially. Using the methodology described previously, it is possible to decompose the domains into regions of varying elastic modulus, as shown in Figure 5. Even before deformation, clear regions of relatively high and low modulus are present, demonstrating that materials normally considered as a continuous bulk in fact exhibit some degree of heterogeneity in their local mechanical properties, as has been shown in the past.[15]

We first examine the pure polymer systems across the available measures. To connect the measurement of C to cavitation, the positions at which the first well-defined voids appear are overlaid in black dots onto the color maps. Void nucleation sites tend to be localized near regions of lower moduli, but they do not necessarily occur at the global minima in C. Here it is important to emphasize that we are examining the connection between the undeformed bulk and the site of void formation after yield. Despite the evolution of the system under the enhanced mobility of deformation, there remains a distinct connection between C and void nucleation. In other words, local moduli can be used to anticipate where voids will form, and the information about which sites will fail is encoded in the configurations.

As noted previously, outliers in Voronoi volume are a good indicator of voids, and it is of interest to measure how well Voronoi volume itself is correlated with C. As a baseline, we first compare C to the Voronoi volume at equilibrium, obtaining a correlation of -0.217 on a site-by-site basis. This suggests that $\sim$20% of the information about the local mechanical structure is determined by Voronoi volume. Comparing C at equilibrium to the Voronoi volume at yield (i.e., at a strain of 0.08) reveals a negligible correlation of -0.007 on a site-by-site basis. Spatial averaging increases the correlation to -0.021—still a relatively small value. Note, however, that Voronoi volume is not the "voidness" of a site, so a low correlation between C and Voronoi volume does not imply a lack of correlation between C and void character.

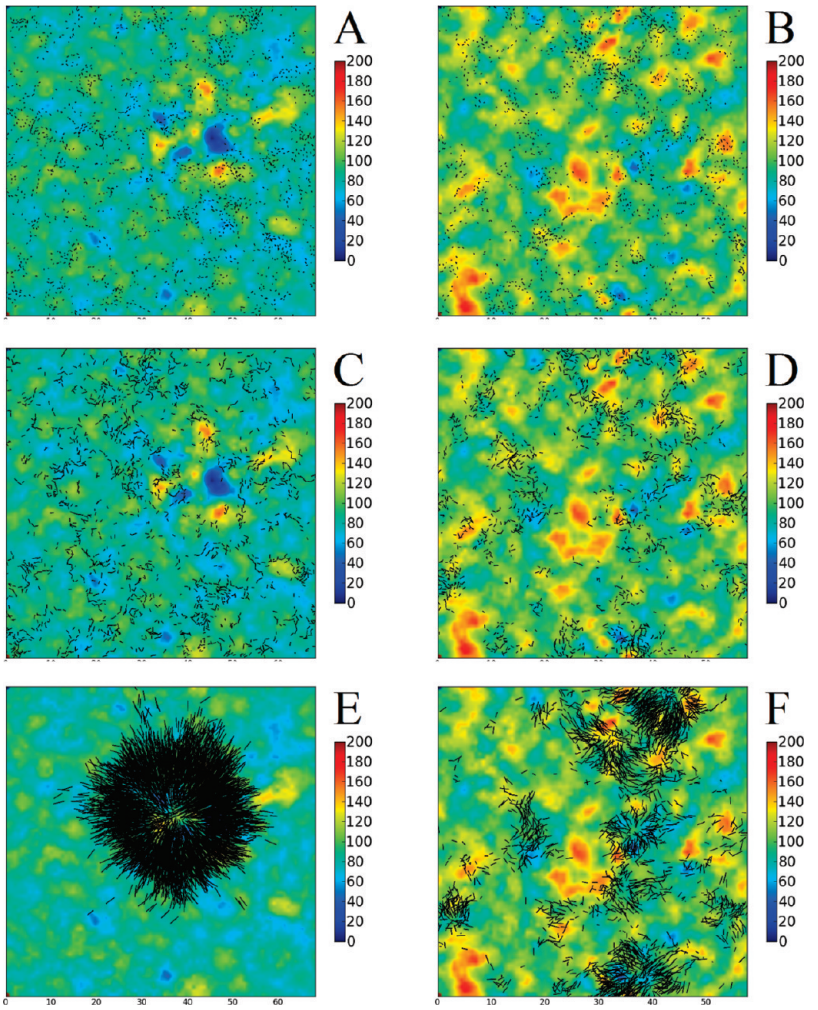

Figure 6. Cross section of local elastic (bulk) modulus corresponding to 4σ thick slices prior to deformation. Images A, C, and E correspond to the pure polymer, and images B, D, and F correspond to the 8-mer nanocomposites. Images are overlaid with the largest 10% of nonaffine displacement vectors. Images A and B are total displacements during 1% deformation, images C and D are displacements immediately before and during the first moments of void formation (over the course of a 1% deformation), and images E and F are total displacements during 10% deformation.

Nonaffine displacements were also examined for their connection to cavitation. In Figure 6, the largest 10% of nonaffine displacements occurring over the course of void nucleation are shown. At the beginning of deformation, the displacements are broadly distributed throughout the polymer with no meaningful correlation to local elastic modulus. Several "strings" of correlated displacements are visible in the pure polymer by the time void formation occurs. However, the displacement fields do not immediately reveal the location of these voids, as determined by LVVS. As the deformation progresses, the large nonaffine displacements become concentrated in a smaller fraction of the system. Examination of total nonaffine displacements at higher deformations reveals starburst patterns outlining the growing voids. Unfortunately, nonaffine displacement serves as a poor predictor of void nucleation itself, providing a clear picture only after voids have formed. Correlations between nonaffine displacements and either C or Voronoi volume are smaller than 0.010 (in absolute value).

Calculation of C at the moment of void formation is difficult for the pure polymer case. As part of the C measurement, the energy is first minimized. For pure polymers, shortly after a 6% deformation, voids start forming during these minimizations, even though the system does not develop voids until after 9% deformation. The earliest minimization-induced voids occur at random locations, but as deformation continues, they soon converge onto a common position that coincides with the spatial location of the eventual true void.

Recall from Figure 2 that the distribution of Voronoi volumes corresponding to nonvoid sites (e.g., the Gaussian part) increased during deformation until voids began to form. Once cavitation began, the distribution for nonvoid sites decreased back to the value it had at 6% deformation. This suggests that the distribution at 6% represents the stable distribution of Voronoi volume during deformation, and the "overshoot" occurring between 6% and 10% is caused by the difficulty to nucleate a void. Interestingly, the appearance of minimization-induced voids corresponds to the strain at which that "overshoot" first began.

We now turn to consideration of the PNC systems. Examination of the Voronoi volume for PNCs in Figure 7 shows the same Gaussian distribution and eventual development of a non-Gaussian tail that is seen in the pure polymers. There are, however, some notable differences. First, the onset of void formation occurs at a lower strain. Second, the "overshoot" in Voronoi

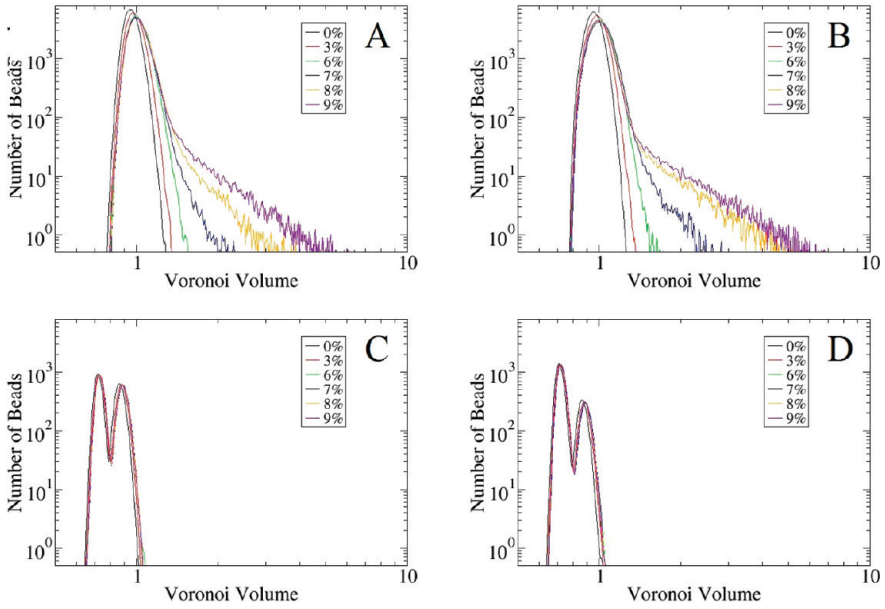

Figure 7. Distribution of Voronoi volume in polymer nanocomposites during triaxial deformation at a rate of 1.2×10^{-4}: (A, C) 4-mer PNCs; (B, D) 8-mer PNCs. (A) and (B) correspond to the polymer components of the systems, and (C) and (D) correspond to the particle components.

volume of nonvoid beads seen in the pure polymer does not occur. Instead, the distribution describing the majority of beads does not change after the tail begins to form. Unlike the pure polymer, PNCs do not develop minimization-induced voids. Taken together, the changes imply that a void forms in the PNC system almost as soon as it is thermodynamically favorable, while for the pure polymers additional energy is required to overcome an energetic barrier.

The Voronoi volume of the rods in the PNCs was also measured during deformation; results are shown in Figure 7. Here a bimodal distribution is visible due to the looser packing near the ends of the rods as compared to the inner beads. Otherwise, the figures are remarkable for the lack of change that occurs during deformation. As can be seen, nanoparticles avoid the cavities well into void development.

In contrast to the tendency of pure polymer systems to be dominated by a single void, the PNC systems show the spontaneous generation of several voids in rapid succession around 6.5%. By around 7%, the number of voids in the system has stabilized, and the existing voids slowly grow until the images in Figure 3 are produced. After a small population of voids is established, no additional voids are nucleated as the existing cavities take on additional volume. While voids first appear later for the pure polymer system, around 9%, both pure polymer and PNC systems have similar total void volumes by around 10%, owing to the faster initial void growth in the pure polymer case. The images in Figure 3 reinforce the concept that void formation is dynamically easier in the PNCs than in the pure polymer.

Returning to Figure 5, it is evident that a strong correlation exists between rod position and local elastic modulus, as the inclusions often coincide with regions of high modulus. Note that in the images presented only the local elastic constants of the polymer component are used to generate the color maps. This allows us to clearly see that improvement in mechanical properties is induced by the attractive additives, beyond their own inherent strength. This result is consistent with our previous examination of fillers.[17] The correlation between local rod concentration and high polymer C is robust, with a value of 0.456 for the 8-mer and 0.065 for the 4-mer, as measured by spatial averages over the variables. In the 8-mer PNCs, some polymer becomes trapped within rod clusters, and these intercalated polymers have high C. The 4-mer PNCs are more uniformly dispersed and do not trap polymer chains in this fashion, resulting in a weaker correlation between local rod concentration and C.

Examination of nonaffine displacements in the PNCs reveals that larger displacements are more likely to occur in regions of lower rod concentration, as shown in Figure 6. The correlation between rod concentration and the magnitude of nonaffine displacement on a site-by-site basis shows no real connection by the time voids occur, with correlations of 0.023 for the 8-mer and −0.010 for the 4-mer. After cavitation has occurred, it is possible to see some regions of overall flow that precede crazing. However, despite the limited visual appearance of connection between equilibrium C and nonaffine displacement, direct measures of correlation return absolute values smaller than 0.010.

Having established that local mechanical stiffness is clearly related to rod position, we now turn to the relationship between Voronoi volume and C for PNCs. Voronoi volume prior to deformation has a correlation with C of −0.256 for the 8-mer and −0.230 for the 4-mer, similar to the pure polymer. However, Voronoi volume at the point of void formation has a correlation with C of −0.114 for the 8-mer and −0.077 for the 4-mer. While not large values in and of themselves, it is clear that information encoded in the systems about their C before deformation remains encoded in the systems throughout the deformation process for these PNCs. That correlation remains apparent despite particle movement due to deformation-enhanced mobility.

Polymers pack more effectively around attractive inclusions.[30] One would expect to see a strong correlation between Voronoi volume and local elastic modulus for the PNCs, since the polymeric material near rods is also mechanically stronger. Scatter plots of these data (not shown) exhibit considerable noise, as both Voronoi volume and C are subject to large fluctuations, producing the modest correlations discussed thus far. However,

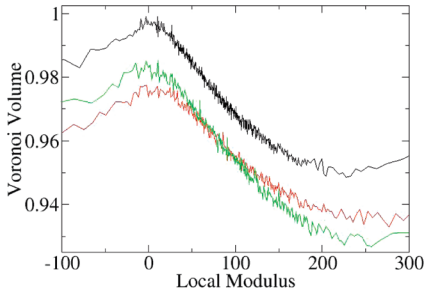

Figure 8. Relationship between Voronoi volume and elastic modulus for each system. The black line represents the pure polymer, the red line represents the 4-mer nanocomposite, and the green line represents the 8-mer nanocomposite.

by smoothing the data over a 1000-point running average, the underlying trend becomes apparent, as seen in Figure 8. Sites with truly high or low C (e.g., outside the range of the plot) are essentially uncorrelated with Voronoi volume. The lack of correlation in the tail values as well as the general noise at typical values account for the low Pearson correlation despite a clear trend for the bulk of the data. A similar connection between Voronoi volume and C was noted previously.[18] Interestingly, this connection is not merely the result of mutual correlation to rod position, as the same trend exists in the pure polymer system as well.

Recall that in the calculation of local stress it was necessary to divide by a local volume; the Voronoi volume from the minimized state was used in this study. To demonstrate that the connection between C and Voronoi volume shown in Figure 8 is not the result of the local stress definition used here, an alternative C was also calculated. This second calculation was performed using the average volume per site, defined as the total system volume divided by the total number of sites. This change produced only a minor shift in the line (not shown), indicating that the relationship between C and Voronoi represents a meaningful connection. The lack of a change is partially due to how small the relative differences in local volume actually are. As such, low Voronoi volume itself is an indicator of high local mechanical stiffness.

Since higher Voronoi volume is correlated to lower mechanical stiffness, LVVS would be expected (at equilibrium) to be mechanically weaker than other sites in the system. The question arises as to whether early LVVS correspond to sites of eventual void formation. To examine this question, we first measure the fraction of all sites that are LVVS during the cavitation process, shown in Figure 9. Here the lines for each system are shown explicitly, rather than being averaged together. For all systems, there are few LVVS prior to deformation, but the population grows exponentially when the material is deformed. This is the result of the Gaussian tail of the distribution slowly drifting to higher values. For the PNCs, there is a transition to a linear regime (abruptly for 8-mer, smoothly for 4-mer) above 7% strain, corresponding to void formation. For the pure polymer, however, the transition to the linear regime is preceded by a sharp drop in the number of LVVS sites, corresponding to the relaxation in the nonvoid Voronoi volume distribution mentioned before.

From the beginning of the linear regime onward, the identity of LVVS sites does not change with time. A question that arises then is, what connection do the stable voids have with equilibrium

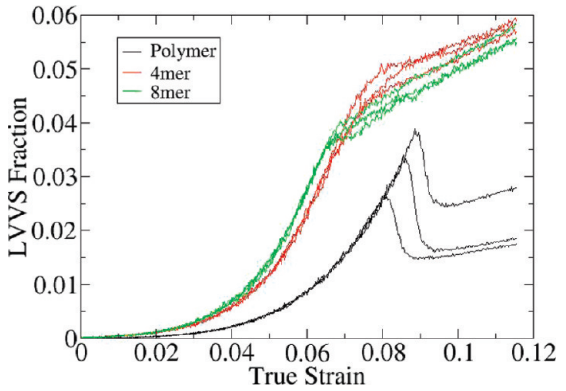

Figure 9. Fraction of sites whose Voronoi volume is larger than 1.2 during triaxial deformation at a rate of 1.2×10^{-4}. Results from several individual realizations are shown directly without averaging over configurations.

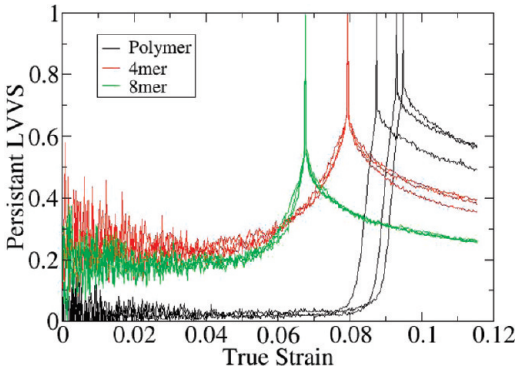

Figure 10. Fraction of LVVS that are part of the first developed void structure as a function of strain during triaxial deformation at a rate of 1.2×10^{-4}. Results from several individual realizations are shown directly without averaging over configurations.

and early deformation LVVS? Figure 10 shows the fraction of LVVS sites at a given time that are also part of the initial stable void at the beginning of the linear regime. In the PNCs, around 25% of the early LVVS correspond to sites in the final void. In other words, despite fluctuations of LVVS at low strains, the information about which sites can fail is encoded in the original configuration at rest. In contrast, for the pure polymers, however, there is no connection between stable void sites and early LVVS. Looking at all sites, the correlation between Voronoi volume at equilibrium and at void formation is 0.399 for the 4-mer and 0.454 for the 8-mer. However, a much smaller correlation exists in the pure polymer case, with a value of 0.041. This suggests that the nature of void formation in PNCs is fundamentally different from that in pure polymer systems.

The results presented above, all generated at a deformation rate of 1.2×10^{-4}, suggest that void formation is dynamically easier in the PNCs than in the pure polymer. As such, it would follow that a large change in deformation rate will alter the time available for local relaxation and hence the nature of void formation observed. To test this hypothesis, the pure polymer and the 4-mer systems were each subjected to deformation rates 10 times faster and 10 times slower. The stress−strain response of these systems is shown in Figure 11. Increasing the rate of deformation drastically moves the stress peak corresponding to

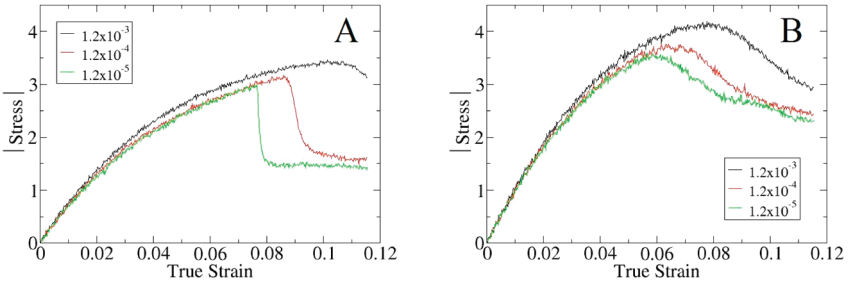

Figure 11. Triaxial deformation at various deformation rates. The pure polymer is shown in panel A, and the 4-mer is shown in panel B. One realization of each system shown directly without averaging.

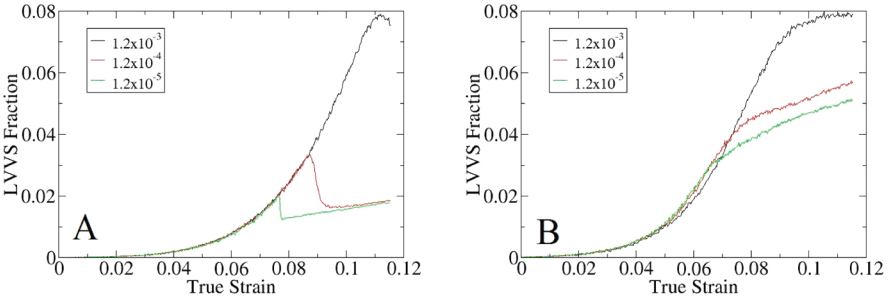

Figure 12. Fraction of sites whose Voronoi volume is larger than 1.2 during triaxial deformation at various deformation rates. The pure polymer is shown in panel A, and the 4-mer is shown in panel B. Results are shown for only one realization for each system, without averaging over realizations.

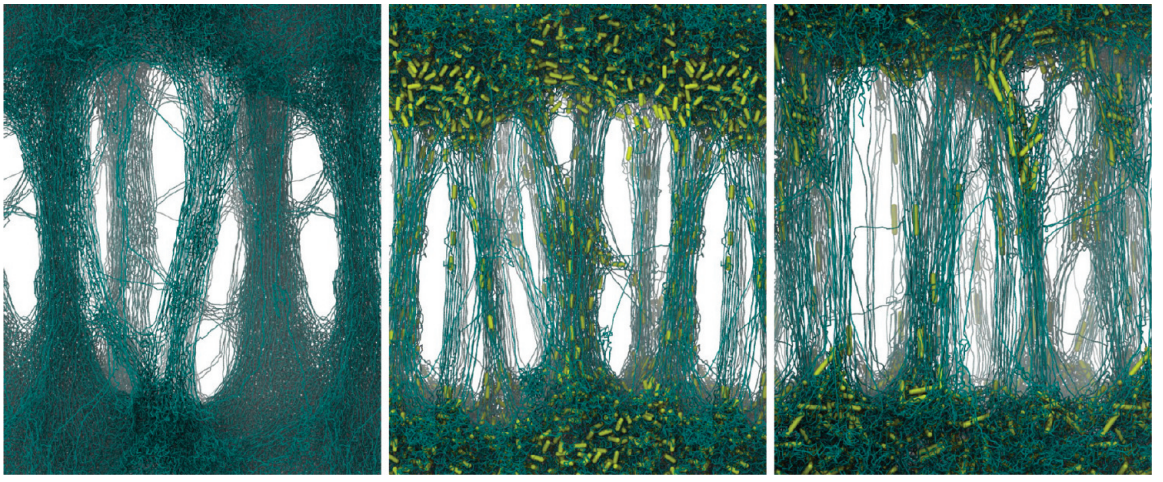

Figure 13. Visualization of craze fibrils in pure polymer and PNC systems. The image on the left represents a pure polymer system, the image in the center represents a 4-mer system, and the image on the right represents an 8-mer system. The nanorods are shown in yellow, and cyan lines denote the polymer chains.

void formation to higher strains; it also increases stress throughout the deformation. Slower deformations allow void formation to occur at lower strains, as the system has more time to nucleate favorable voids.

In Figure 12, the fraction of sites that qualify as LVVS is shown during the course of deformation. For the pure polymer, the LVVS fraction does not depend upon deformation rate until void formation causes a sudden drop. After voids have formed, it can be seen that the slower two rates approach a similar LVVS fraction. In contrast, examination of the 4-mer PNCs instead reveals that LVVS have a weak dependence upon deformation rate even before void formation. After void formation, the 4-mer PNCs curves have similar slopes but exhibit a larger offset between each other than was observed for the pure polymers.

PREMATURE CRAZING

After voids have formed in a system, they slowly grow while generally maintaining their spherical shape. Eventually, these voids begin to influence one another and percolate into one or more large, irregularly shaped spaces across which strands of polymeric material are held. For chains whose size exceeds some characteristic length scale, presumably the entanglement length,[2] these polymer strands are not able to clear the forming supervoid

despite the large stress being placed upon them. The visual appearance of these premature crazes can be appreciated in Figure 13. The forming polymeric fibrils rarely consist of a single chain, but rather form in small clusters. The width of fibrils and spacing between adjacent fibrils is essentially random, as previously noted.[6]

The pure polymer systems behave differently than the PNC systems in many respects. As noted before, for the pure polymer a single large void usually dominates the early cavitation process. Additional voids form before the primary void approaches the length scale of the box and then grow disproportionately faster achieving similar size as the original void. At this point, the void begins to lengthen along the axis of deformation and a craze structure is developed. Although multiple fibrils of material exist, it is possible to distinguish the individual voids well into the crazing. This is distinctly different from the PNCs, where percolation of smaller voids allows a plane of failure to arise, across which well-defined fibrils are established early on.

Prior to deformation, the rods are oriented at random throughout the system. During the early void formation process, the orientation of the rods remains unchanged; in fact, they are locally frozen in place. Once the crazes begin to form, two distinct populations of rods exist. The first set is those in the bulk that have not been displaced and retain their globally random orientation. The second set is those which became trapped within the percolating void structure and become incorporated into the early fibrils. These rods align strongly with the direction of the polymer fibril to which they are attached, even in cases when the fibril itself is not aligned parallel to the axis of deformation. Figure 14 shows the degree of rod alignment with the axis of deformation, where P_x is the second Legendre polynomial of the rod end-to-end vector dotted into the unit x vector (e.g., the direction of deformation). A value of zero indicates random orientation, and a value of unity denotes perfect alignment.

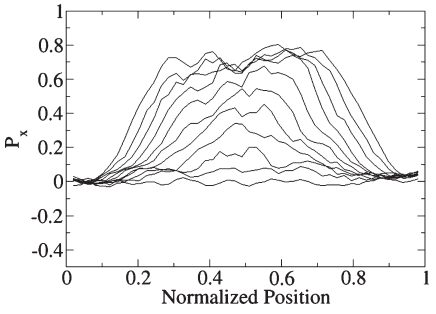

Figure 14. Rod alignment with respect to the axis of deformation during craze development for 4-mer. The lines progress from the undeformed system (bottom line) to completed craze (top line).

As the craze develops, new polymer and nanorods are drawn into the fibrils. Rods reorient themselves along the fibril axes as this occurs. Examination of the surface layer of rods at the interface of the bulk and fibrils shows they also have a random orientation. That is, there is no depletion of parallel rods (as one might expect if incorporation of new rods into the fibril was alignment dependent), nor is there a higher degree of parallel alignment (in the case of there being some type of gradient of alignment at the interface). Instead, it appears that realignment and incorporation into the fibril region occur simultaneously.

Lastly, it is particularly instructive to discuss the overall distribution of material in the premature crazes by examining the local density in "slices" of material along the axis of deformation, as seen in Figure 15. From this information, it is possible to determine the stretching ratio, given by

$$\lambda = \frac{\rho_{\text{bulk}}}{\rho_{\text{craze}}} \tag{5}$$

where ρ_{bulk} is the density in the bulk and ρ_{craze} is the density in the crazed region of the sample. Using eq 4, the entanglement length, N_e, can be calculated from λ directly. For the pure polymer, we determine $\lambda = 5.6 \pm 0.3$, which is in agreement with results for flexible chains examined by Rottler and Robbins.[6] This corresponds to an entanglement length of 49 ± 3, which is slightly below the value of 56.0 ± 3.5 that we obtained from a direct topological analysis of the bulk system using a contact definition.[19] The λ of the PNCs is measured twice using two approaches. First we consider only the polymer component, and second we include both the polymer and the particles. For the 4-mer, λ is 8.2 ± 0.2 or 8.3 ± 0.2, based on the polymer only and both polymer and particles, respectively. For the 8-mer, λ is 9.4 ± 0.2 or 10.4 ± 0.2, based on the polymer only and both polymer and particles, respectively. Again using eq 4, it is found that N_e ranges from 96 to 173 depending on the particular system and the approach used to determine λ.

The entanglement molecular weight of these PNC systems was previously examined by direct topological analysis.[19] Depending on the specific details of the entanglement calculation procedure, the resulting N_e can vary significantly. However, in all cases the N_e of a PNC is either equal to or smaller than the N_e of the corresponding pure polymer. This is in contradiction with the N_e calculated here for PNCs from λ according to eq 4. This suggests that the simple cross-linking model upon which eq 4 is based does not remain valid for nanocomposite materials. Note

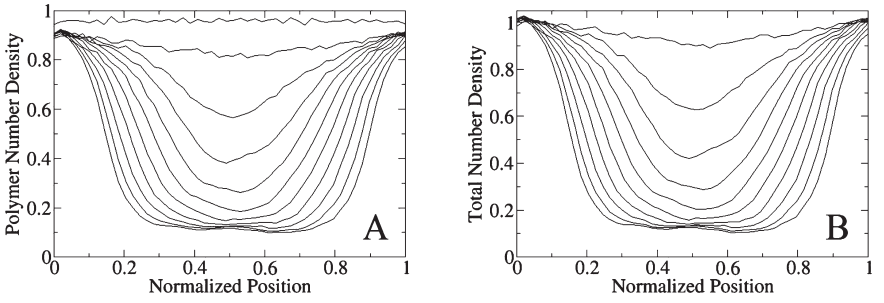

Figure 15. Local density during crazing of the 4-mer polymer component only (A) and the total system (B). The lines progress from the undeformed system (top line) to completed craze (bottom line). Distances are normalized by the length of the simulation box, which varies considerably during crazing.

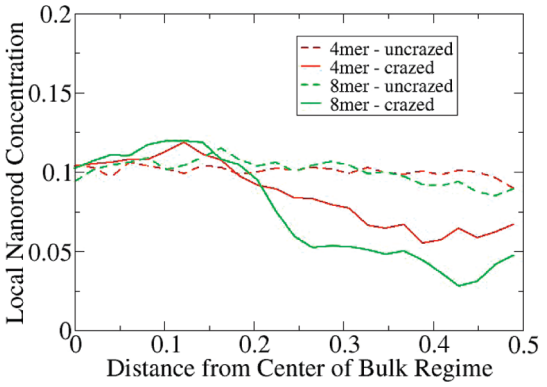

Figure 16. Local concentration of nanorods before and after crazing.

that recent calculations of PNCs under deformation demonstrated that cross-linking models also fail to explain hardening modulus.[20]

From the density information, it is also possible to examine the local concentration of nanorods. The bulk concentration of rods for all PNC systems was 10 wt % nanorods. The error in local concentration measurements is nearly 1%, due to the small number of rods in a given slice. In the premature crazes, the 4-mer systems have a concentration of nanorods in the fibrils of ∼7 wt %, which is notably different than the undeformed bulk concentration. In the 8-mer systems the nanorod concentration in the crazed region is closer to 5 wt %. The lower concentration of rods in the fibrils is accompanied by a notable increase in concentration at the fibril−bulk interface to 12 wt % for the 8-mer and 11.5 wt % for the 4-mer. These results suggest that attractive additives resist incorporation into the forming crazes, consistent with the experimental observations of Lee et al.[12] Furthermore, this effect causes an accumulation of rods at the base of the fibrils and drives an increase in local concentration in the remaining bulk phase, which is most notable at the interface between the two domains. Changes in concentration are more notable for larger additives.

CONCLUSION

Multiaxial stress induces the formation of voids and eventual crazing of polymeric materials. The introduction of attractive rodlike additives fundamentally changes how these voids form and the structure of premature crazes.

For the pure polymer system, a number of distinct phenomena stand out. Upon the application of multiaxial stress, additional volume is forced into the polymeric samples. At low strains, this volume is distributed across all sites of the system. For the pure polymer, the abrupt nucleation of a single void allows the majority of the system to relax to smaller local volumes. When systems pertaining to the Voronoi volume distribution "overshoot" are minimized, they spontaneously form voids, suggesting that cavitation has become thermodynamically favorable but is not yet able to nucleate large regions. The appearance of voids is correlated with regions of low elastic modulus prior to deformation, thereby providing a distinct local property that can be used to predict sites of failure. In contrast, nonaffine displacements do not exhibit a predictive quality but are correlated with void location after the onset of cavitation. The above observations, particularly the onset of void formation, are strongly deformation rate dependent.

The addition of nanorods to the polymers changed the cavitation and crazing behaviors considerably. In the PNCs, multiple voids form simultaneously and at lower strains than in the pure polymers. As such, the PNCs never exhibit the "overshoot" in Voronoi volume distributions experienced by the pure polymers. This difference in behavior is driven by the comparatively larger mechanical heterogeneity seen in the PNCs, which helps localize early void formation to predictable regions of polymer far from the nanorod inclusions; such regions have generally lower local elastic modulus. As in the pure polymers, the PNC elastic moduli are correlated with local Voronoi volume. However, this correlation persists during deformation, beyond yield. Additionally, it is found that ∼25% of sites with a Voronoi volume above 1.2 during early deformation are part of the initial stable voids. As such, the location of void nucleation can be predicted for nanocomposite materials from Voronoi volumes as well as from local moduli.

By understanding the differences in the cavitation states of the systems, it is easier to account for differences in early craze formation. Specifically, the percolation of multiple smaller voids in PNCs leads to scattered initial craze regions wherein small pockets of additives can become trapped. Once crazes begin to grow, it is clear that the growing fibrils resist the incorporation of additional nanorods, especially for the larger inclusions considered here. The combination of reluctant additive incorporation and early trapped pockets is in agreement with experimental observations of Lee et al.[12]

The stretching ratios observed here for pure polymers are in good agreement with previous work.[6] When applied to the PNCs, however, the use of simple cross-link models to further predict entanglement length returned values larger than those found for the pure polymer. Furthermore, such values are inconsistent with more detailed measurements of entanglement length reported in recent work.[19]

Overall, the addition of nanoparticles drastically changes the behavior of cavitation and crazing in polymeric materials. Despite fluctuations of the number of large Voronoi volume sites at low strains, the information about which sites can fail is encoded in the configuration. While nanorod inclusions increase the overall strength of the material,[20] they also make the transition toward failure easier, in part due to the more heterogeneous environment they create. Once failure begins via crazing, these additives resist incorporation into fibrils. Such a process is shape and size dependent. This complex picture suggests that considerable information about the nuances of PNC craze systems remains to be uncovered.

AUTHOR INFORMATION

Corresponding Author

*E-mail: depablo@engr.wisc.edu.

ACKNOWLEDGMENT

We thank the Grid Laboratory of Wisconsin (GLOW) for use of their computation resources and Chi-cheng Chiu for visualization of crazed systems. This material is based upon work supported by the Department of Energy under Award Number DE-SC0004025.

REFERENCES

(1) Mahajan, D.; Singh, B.; Basu, S. Void nucleation and disentanglement in glassy amorphous polymers. *Phys. Rev. E* **2010**, *82*, 11803.

(2) Baljon, A.; Robbins, M. Simulations of crazing in polymer glasses: Effect of chain length and surface tension. *Macromolecules* **2001**, *34*, 4200–4209.
(3) Sixou, B. Molecular dynamics simulation of the first stages of cavitation process in amorphous polymers. *Mol. Simul.* **2007**, *33*, 965–973.
(4) Kramer, E.; Berger, L. Fundamental processes of craze growth and fracture. *Crazing Polym.* **1990**, *2*, 1–68.
(5) Estevez, R.; Tijssens, M.; Van der Giessen, E. Modeling of the competition between shear yielding and crazing in glassy polymers. *J. Mech. Phys. Solids* **2000**, *48*, 2585–2617.
(6) Rottler, J.; Robbins, M. Growth, microstructure, and failure of crazes in glassy polymers. *Phys. Rev. E* **2003**, *68*, 11801.
(7) Akcora, P.; Kumar, S. K.; Moll, J.; Lewis, S.; Schadler, L. S.; Li, Y.; Benicewicz, B. C.; Sandy, A.; Narayanan, S.; Illavsky, J.; Thiyagarajan, P.; Colby, R. H.; Douglas, J. F. "Gel-like" Mechanical Reinforcement in Polymer Nanocomposite Melts. *Macromolecules* **2010**, *42*, 1003–1010.
(8) Komarneni, S. Nanocomposites. *J. Mater. Chem.* **1992**, *2*, 1219–1230.
(9) Kamel, S. Nanotechnology and its applications in lignocellulosic composites, A mini review. *eXPRESS Polym. Lett.* **2007**, *1*, 546–575.
(10) Huang, Z. M.; Zhang, Y. Z.; Kotaki, M.; Ramakrishna, S. A review on polymer nanofibers by electrospinning and their applications in nanocomposites. *Compos. Sci. Technol.* **2003**, *63*, 2223–2253.
(11) Gangopadhyay, R.; De, A. Conducting polymer nanocomposites: a brief overview. *Chem. Mater.* **2000**, *12*, 608–622.
(12) Lee, J.; Zhang, Q.; Emrick, T.; Crosby, A. Nanoparticle alignment and repulsion during failure of glassy polymer nanocomposites. *Macromolecules* **2006**, *39*, 7392–7396.
(13) Bagheri, R.; Pearson, R. Role of particle cavitation in rubber-toughened epoxies: 1. Microvoid toughening. *Polymer* **1996**, *37*, 4529–4538.
(14) Gersappe, D. Molecular mechanisms of failure in polymer nanocomposites. *Phys. Rev. Lett.* **2002**, *89*, 58301.
(15) Yoshimoto, K.; Jain, T.; Workum, K.; Nealey, P.; de Pablo, J. Mechanical heterogeneities in model polymer glasses at small length scales. *Phys. Rev. Lett.* **2004**, *93*, 175501.
(16) Buryachenko, V.; Roy, A.; Lafdi, K.; Anderson, K.; Chellapilla, S. Multi-scale mechanics of nanocomposites including interface: experimental and numerical investigation. *Compos. Sci. Technol.* **2005**, *65*, 2435–2465.
(17) Papakonstantopoulos, G.; Yoshimoto, K.; Doxastakis, M.; Nealey, P.; de Pablo, J. Local mechanical properties of polymeric nanocomposites. *Phys. Rev. E* **2005**, *72*, 31801.
(18) Papakonstantopoulos, G.; Riggleman, R.; Barrat, J.; de Pablo, J. Molecular plasticity of polymeric glasses in the elastic regime. *Phys. Rev. E* **2008**, *77*, 41502.
(19) Toepperwein, G. N.; Karayiannis, N.; Riggleman, R.; Kröger, M.; de Pablo, J. Influence of Nanorod Inclusions on Structure and Primitive Path Network of Polymer Nanocomposites at Equilibrium and Under Deformation. *Macromolecules* **2011**, *44*, 1034–1045.
(20) Toepperwein, G. N.; Riggleman, R. A.; de Pablo, J. J. Dynamics and Deformation Response of Rod-Containing Nanocomposites, manuscript in preparation.
(21) Sides, S. W.; Grest, G. S.; Stevens, M. J.; Plimpton, S. J. Effect of end-tethered polymers on surface adhesion of glassy polymers. *J. Polym. Sci., Part B* **2004**, *42*, 199–208.
(22) de Pablo, J. J.; Laso, M.; Suter, U. W. Simulation of polyethylene above and below the melting point. *J. Chem. Phys.* **1992**, *96*, 2395.
(23) Banaszak, B. J.; de Pablo, J. J. A new double-rebridging technique for linear polyethylene. *J. Chem. Phys.* **2003**, *119*, 2456.
(24) http://math.lbl.gov/voro++/.
(25) Bitzek, E.; Koskinen, P.; Gahler, F.; Moseler, M.; Gumbsch, P. Structural relaxation made simple. *Phys. Rev. Lett.* **2006**, *97*, 170201.
(26) Zhou, M. A new look at the atomic level virial stress: on continuum-molecular system equivalence. *Proc. R. Soc. London, Ser. A* **2003**, *459*, 2347.
(27) Falk, M.; Langer, J. Dynamics of viscoplastic deformation in amorphous solids. *Phys. Rev. E* **1998**, *57*, 7192–7205.
(28) Riggleman, R.; Lee, H.; Ediger, M.; Pablo, J. Heterogeneous dynamics during deformation of a polymer glass. *Soft Matter* **2010**, *6*, 287–291.
(29) Ward, I. *Mechanical Properties of Solid Polymers*; John Wiley & Sons Ltd.: Chichester, 1983; Chapter 12.
(30) Vacatello, M. Monte Carlo simulations of polymer melts filled with solid nanoparticles. *Macromolecules* **2001**, *34*, 1946–1952.
(31) Makke, A.; Perez, M.; Rottler, J.; Lame, O.; Barrat, J. L. Predictors of cavitation in glassy polymers under tensile strain: a coarse grained molecular dynamics investigation. Manuscript in press.

NOTE ADDED IN PROOF

Recently, Makke et al. have performed simulations of cavitation for a coarse-grained polymer model that is similar to the one employed in this work. Consistent with the results described here, these authors find that for pure polymers the formation of voids is correlated with local elastic moduli of the material.[31]